NuSTAR as an Axion Helioscope

J. Ruz,[1,2,*] E. Todarello,[3,4,5,†] J. K. Vogel,[1,2,‡] F. R. Candón,[1,2] M. Giannotti,[2,6] B. Grefenstette,[7] H. S. Hudson,[8] I. G. Hannah,[8] I. G. Irastorza,[2] C. S. Kim,[9] M. Regis,[4,5] D. M. Smith,[10] M. Taoso,[5] and J. Trujillo Bueno[11,12]

[1]*Fakultät für Physik, Technische Universität Dortmund, Dortmund, D-44221, Germany*
[2]*Centro de Astropartículas y Física de Altas Energías, University of Zaragoza, Zaragoza, 50009, Spain*
[3]*School of Physics and Astronomy, University of Nottingham, University Park, NG7 2RD, Nottingham, United Kingdom*
[4]*Dipartimento di Fisica, University of Torino, I-10125, Torino, Italy*
[5]*Istituto Nazionale di Fisica Nucleare, Sezione di Torino, I-10125, Torino, Italy*
[6]*Department of Chemistry and Physics, Barry University, Miami Shores, 33161, Florida, USA*
[7]*California Institute of Technology, Space Radiation Lab, Pasadena, 91125, California, USA*
[8]*School of Physics and Astronomy, University of Glasgow, Glasgow, G12 8QQ, Scotland, United Kingdom*
[9]*Department of Physics, University of California Santa Barbara, Santa Barbara, 93106, California, USA*
[10]*Physics Department and Santa Cruz Institute for Particle Physics, University of California Santa Cruz, Santa Cruz, 95064, California, USA*
[11]*Instituto de Astrofísica de Canarias, La Laguna, 38205, Tenerife, Spain*
[12]*Consejo Superior de Investigaciones Científicas, E-28006 Madrid, Spain*

(Received 9 December 2024; revised 25 June 2025; accepted 19 August 2025; published 2 October 2025)

We present a novel approach to investigating axions and axionlike particles by studying their potential conversion into x-rays within the Sun's atmospheric magnetic field. Utilizing high-sensitivity data from the nuclear spectroscopic telescope array (NuSTAR) collected during the 2020 solar minimum, along with advanced solar atmospheric magnetic field models, we establish a new limit on the axion-photon coupling strength $g_{a\gamma} \lesssim 7.3 \times 10^{-12}$ GeV^{-1} at 95% CL for axion masses $m_a \lesssim 4 \times 10^{-7}$ eV. This constraint surpasses current ground-based experimental limits, studying previously unexplored regions of the axion-photon coupling parameter space up to masses of $m_a \lesssim 3.4 \times 10^{-4}$ eV. These findings mark a significant advancement in our ability to probe axion properties and strengthen indirect searches for dark matter candidates.

DOI: 10.1103/18sn-hxtb

Introduction—The standard model (SM) of particle physics has provided a remarkably successful framework for describing the fundamental particles and their interactions via three of the four known fundamental forces. Despite its predictive power, the SM leaves several key questions unresolved, notably the strong charge-parity (CP) problem in quantum chromodynamics (QCD) and the composition of dark matter. Intriguingly, a single theoretical extension proposed over four decades ago by Peccei and Quinn [1] offers a potential solution to both. This framework predicts the existence of a light, pseudoscalar boson—the QCD axion [2–7]. Beyond this minimal realization, a broader class of particles known as axionlike particles (ALPs) [8] arises in many extensions of the SM. Like QCD axions, ALPs are pseudoscalar bosons that couple to photons, but unlike QCD axions, they are not constrained by a specific relationship between their mass m_a and the Peccei-Quinn symmetry-breaking scale f_a. Although ALPs do not solve the strong CP problem, they remain compelling candidates for dark matter. For the purposes of this Letter, we will refer to both QCD axions and ALPs generically as "axions."

Numerous laboratory and astronomical experiments have been carried out to detect axions [9–39], with additional efforts either ongoing or proposed [31,40–42]. These investigations predominantly focus on the interaction of axions with photons [43], described by the effective Lagrangian term $\mathcal{L}_{a\gamma} = g_{a\gamma}\mathbf{E} \cdot \mathbf{B}a$, where a represents the axion field, $\mathbf{E}$ and $\mathbf{B}$ denote electric and magnetic fields, respectively, and $g_{a\gamma}$ is the coupling strength. Such an interaction enables the Primakoff effect, where photons convert into axions (and vice versa) in the presence of an electromagnetic field.

The Sun acts as a bright source of axions, which are generated in its core via the Primakoff process, wherein

*Contact author: Jaime.Ruz@cern.ch
†Contact author: elisa.todarello@nottingham.ac.uk
‡Contact author: Julia.Vogel@cern.ch

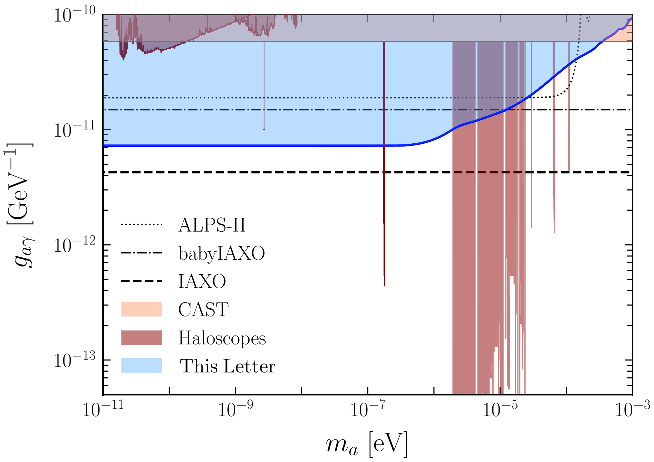

FIG. 1. NuSTAR's 95% CL, exclusion on axion-photon coupling strength $g_{a\gamma}$ (blue line). Regions excluded by this Letter are shown in shaded blue. We present our results in comparison to current [10–39] and future [31,40–42] laboratory experiments.

thermal photons are converted into axions through interactions with the electric fields of electrons and ions in the plasma. These axions can then reconvert into photons within the Sun's atmospheric magnetic fields, yielding a distinct x-ray flux with spectral and spatial characteristics that allow differentiation from typical solar x-ray emissions and background signals in x-ray telescopes. Advances in solar x-ray observational capabilities, such as higher resolution and sensitivity, have improved prospects for identifying solar-origin axions. Initial efforts using satellite instruments for axion detection include the *Yohkoh*/SXT [44] mission data from 1991–2001, utilized in [45] to establish early constraints on the axion-photon coupling. Later missions, including RHESSI [46,47] and *Hinode*/XRT [48], applied similar methodologies, gradually refining observational techniques and constraints on axion interactions. However, due to the high background rates and optimization of these instruments for bright solar x-rays, dedicated solar missions are not optimized for weak-signal dark-matter searches.

In this Letter, we present the first analysis of solar observation x-ray data from NASA's nuclear spectroscopic telescope array (NuSTAR) [49], specifically aimed at searching for signatures of solar axion conversion in the solar atmosphere. We find no evidence for an axion-induced signal above the expected background, allowing us to place stringent constraints on the axion-photon coupling over a significant region of parameter space. In particular, we constrain the axion-photon coupling $g_{a\gamma}$ to less than $7.3\times10^{-12}\ \mathrm{GeV}^{-1}$ at the 95% confidence level (CL) for axion masses $m_a \lesssim 4\times10^{-7}$ eV, substantially improving upon previous limits set by laboratory-based experiments [9–39], exceeding the results of planned experiments [31,40–42] and competing with current astrophysical limits [50–68]. Figure 1 shows the outcome of the present Letter in comparison to those from previous and forthcoming ground-based axion experiments.

Axion conversion in solar atmospheric magnetic field—Accurate theoretical models for the solar axion flux are well established, and our analysis is grounded in the results presented in [69,70]. Since both, the generation of axions from x-rays in the solar core and their reconversion into photons in the solar atmosphere's magnetic field occur via the Primakoff process, the resulting x-ray signal detected by satellite missions scales with $g_{a\gamma}^4$. Axions generated in the core are highly relativistic and follow approximately radial trajectories to the solar surface. The probability of their conversion into photons is then provided by [71]

$$P_{a\to\gamma}(E,h,m_a) = \left(\frac{1}{4}g_{a\gamma}^2\right)\left|\int_0^h dh' B_\perp(h') e^{i\int_0^{h'} dh'' q(h'',m_a)} e^{-\frac{1}{2}\int_{h'}^{h} dh'' \Gamma(h'')}\right|^2, \tag{1}$$

where h is the altitude above the visible surface of the Sun, $B_\perp$ is the component of the magnetic field perpendicular to the direction of propagation of the photon, and $q(h,m_a) = (\omega_p^2(h) - m_a^2)/2E$ is the momentum exchanged between the photon in the medium and the axion, both carrying energy E. The plasma frequency of the medium is $\omega_p(h) = \sqrt{e^2 n_e(h)/m_e}$, where e and m_e are the electric charge and mass of the electron, respectively, while $n_e(h)$ is the height-dependent number density of free electrons plus that of bound electrons with ionization energy much smaller than the x-ray energy. Notably, in natural units, the plasma frequency corresponds to an effective photon mass. The term containing Γ represents the absorption between altitudes h' and h of the arising x-rays in the solar atmosphere [71,72].

In this Letter, we characterize the solar magnetic field by means of advanced and realistic magnetohydrodynamics (MHD) simulations that accurately represent the quiet-Sun atmosphere—that corresponds to the conditions for the NuSTAR solar observations used in this Letter. For altitudes below 400 km, we make use of magnetoconvection simulations with small-scale dynamo activity [73] developed with the MURaM radiative MHD code [74,75]. This three-dimensional (3D) model applies periodic boundary conditions in the horizontal plane orthogonal to the solar radius vector at the observed solar disk location. It accurately represents the quiet internetwork regions of the

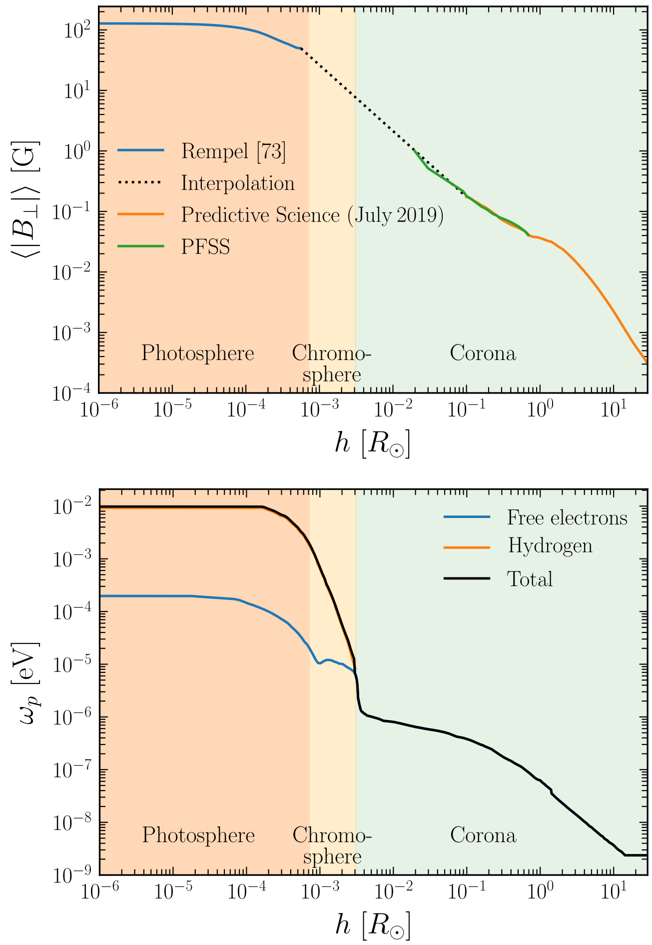

FIG. 2. Modeling of the transverse component of the solar atmospheric magnetic field (top) [73,78], and contributions to axion plasma frequency (bottom) for the photosphere (orange), chromosphere (yellow), and corona (green) regions as function of height in units of the solar radius.

solar photosphere, which cover most of the solar disk across the solar activity cycle. The model's magnetic field, tangled at scales beneath current telescope resolution, shows a mean field strength of 170 G at the visible surface, matching observed depolarization effects in photospheric spectral line polarization [76,77]. The blue curve in the top panel of Fig. 2 illustrates the altitude variation of $\langle|B_\perp|\rangle$, calculated as the spatial average of $|B_\perp|$ across all points in the plane perpendicular to the solar radius vector. For modeling the coronal magnetic field, we utilize the publicly available Predictive Science Inc. (PSI) MHD simulation corresponding to the solar eclipse of July 2, 2019 [78], and apply it to the quiet phase of solar activity of our observations. See Supplemental Material for further details [79]. The PSI simulation provides a 3D representation of the coronal magnetic field up to an altitude of $h = 29R_\odot$. To obtain $\langle|B_\perp|\rangle$, we extract the perpendicular component of the magnetic field relative to the Earth-Sun line of sight, averaged over a disk of radius $0.1R_\odot$ centered on our signal region, as represented by the orange line in the top panel of Fig. 2. We perform a power-law interpolation between the photospheric and coronal magnetic field models (dashed line in the top panel of Fig. 2), which is further validated by the potential-field-source-surface (PFSS) model for the specific day of our observation [96], denoted by the green line in the top panel of Fig. 2.

To accurately calculate the axion-photon conversion probability in the solar magnetic atmosphere, it is essential to model the free electron and hydrogen density. For this purpose, we utilize the model from [97], which is representative of the quiet Sun. This model builds on the VAL-C chromospheric model [98] and the coronal model [99]. Our focus is specifically on the quiet Sun, excluding the added coronal density contributions from the streamer belt. In addition to free electrons and hydrogen, we account for helium (He) in the plasma density, assuming it follows the density profile of hydrogen (H) with a relative abundance $n_{\rm H}/n_{\rm He} = 0.06$ [100–102]. Contributions from heavier elements are not included in the computation of q, as their low abundances render their impact on the plasma frequency negligible. In the chromosphere, where the ionization fraction is low, the plasma frequency is primarily determined by the density of bound electrons in atoms, mainly hydrogen, as shown in the bottom panel of Fig. 2. In the corona, with temperatures on the order of 10^6 K, hydrogen and helium are fully ionized. Given the higher mass of nuclei, their contribution to the plasma frequency is minimal compared to that of free electrons.

The absorption coefficient Γ is calculated as the sum over all species i such that $\Gamma_i = n_i\sigma_i$, where n_i represents the number density of the species i and σ_i is the total photon cross section for that species. We include elements up to atomic number $Z = 30$ in our calculation, using elemental abundances from the CHIANTI database [103,104], specifically based on the Schmelz extended model of coronal abundances derived in [100–102]. For each element, we obtain the total photon cross section from the NIST XCOM database [105], which accounts for x-ray attenuation due to coherent (Rayleigh) and incoherent (Compton) scattering, as well as photoelectric absorption.

NuSTAR observations—On February 21, 2020, NuSTAR was directed toward the center of the solar disk, capturing 23 814 sec of live exposure data with flight module A and 24 983 sec with flight module B, to support both a solar axion search and the analysis of x-ray bright points on the solar photosphere [106]. The minimum of the 11-year solar activity cycle provided a unique opportunity to study the emission from the quiet Sun, and this campaign offers the best data for axion studies, since it involved a long dwell at the disk center during a period of very low solar activity, providing an ideal environment by minimizing interference from bright active regions or solar flares within the $10' \times 10'$ field of view [49]. To identify the predicted axion spectrum, counts were accumulated from pixels within 0.1

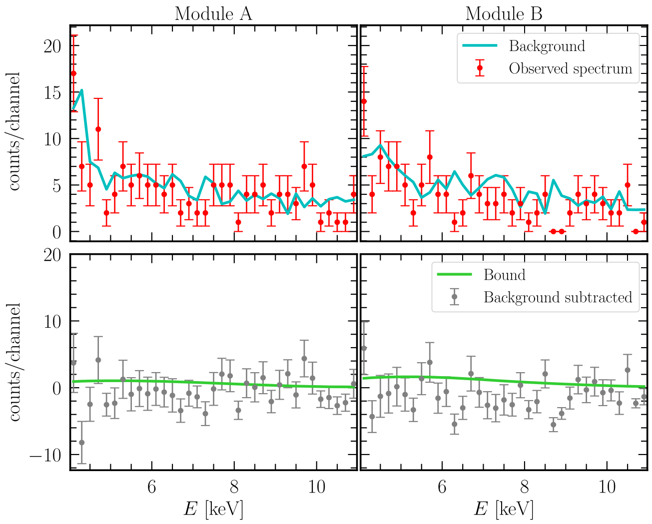

FIG. 3. NuSTAR's observed spectra for module A (left) and B (right) in the signal (red) and area normalized background (cyan) regions. Background-subtracted total spectrum (bottom row) and 95% CL spectral shape of the axion component folded through the instrument response for an exemplary axion mass of $m_a = 10^{-7}$ eV is shown.

solar radii (1.6′) of the disk center, while background counts were gathered from an annulus between 0.15 and 0.30 solar radii.

Although the solar axion surface luminosity profile [107] indicates that an optimal source region for our analysis, given NuSTAR's energy threshold, would be at approximately $0.15R_\odot$, we adopt a more conservative selection radius of $0.1R_\odot$ and account for remaining expected axion signal in the background region as discussed later on in the Analysis Section. This choice satisfies two key criteria: it maximizes the axion flux originating from the solar core while minimizing contamination from bright solar features present during the observation period.

For the analysis presented here, NuSTAR conducted a total of nine observations (orbits). Modules A and B have been analyzed independently, since time exposure, effective area, and detector response are inherent to each particular module. To account for the motion of the solar center in the field of view (FOV), each observation has been divided into four segments, each approximately 700 sec in duration. The top panels of Fig. 3 present the total counts in the signal region as a function of energy (red dots), along with the background (cyan line) derived from the outer annular region for module A (left) and module B (right). The background of the respective modules was adjusted by normalizing to the source area, smoothing via a running polynomial fit, and further correcting for the known gradient of cosmic background x-rays across the detector chips. For clarity, statistical uncertainties of the plotted background were omitted—the detector background was measured over an area 5.3 times larger than the signal region, enhancing the accuracy of background estimation. The bottom panel shows the background subtracted spectrum (gray dots) including error propagation for modules A (left) and B (right) and we report, for illustrative purposes, the expected axion flux (green line) corresponding to the 95% CL of $g_{a\gamma}$ for an axion with mass of 10^{-7} eV. Detailed procedures for the NuSTAR solar data processing using `NASA-HEASARC HEASoft 6.34`, NuSTAR Data Analysis Software (`NuSTARDAS v.2.1.4`) and calibration database (`CALDB v.20240325`) are discussed in Supplemental Material [79]. `XSPEC` tool [108] version 12.13.1 was used to read the spectra and export the data into ASCII format.

Data analysis—The expected photon count resulting from axion conversion within a given NuSTAR energy bin i, originating from region $j = s, b$—where s denotes the signal region ($r < 0.1R_\odot$) and b the background region ($0.15R_\odot < r < 0.3R_\odot$)—is computed separately for each module $k = A, B$ and observation segment as

$$N^{j,k}_{\gamma,i}(h, m_a) = \Delta t^k \int dE A^{j,k}_{\rm eff}(E) \epsilon^k_{{\rm RMF},i}(E) \times \frac{dN^j_a}{dA\, dt\, dE}(E) P_{a\to\gamma}(E, h, m_a), \qquad (2)$$

where Δt^k is the observation exposure and $A^{j,k}_{\rm eff}$ the effective area of a given module k. The energy response function of each telescope in an energy bin i is denoted by $\epsilon^k_{{\rm RMF},i}$ [109]. The term $(dN^j_a/dA\, dt\, dE)(E)$ corresponds to the differential axion flux originating from the solar core, while $P_{a\to\gamma}(E, h, m_a)$ represents the axion-photon conversion probability within the solar atmosphere following Eq. (1). We calculate the total number of photons from axion conversion expected in each module by summing over all the relative segments and account for leftover signal in $0.15 - 0.3R_\odot$. The likelihood analysis was performed using an 80 eV bin width. However, for improved visual clarity, Fig. 3 is presented with a bin width of 200 eV.

The total number of x-ray photons expected in the signal region for a given module and energy bin, is given by

$$\lambda^k_i = N^{s,k}_{\gamma,i}(g^4_{10}) + z^{s,k}_i, \qquad (3)$$

where $z^{s,k}_i$ represents the background of bin i in the signal region and $g_{10} \equiv g_{a\gamma}/10^{-10}$ GeV^{-1}. To estimate $z^{s,k}_i$, we use the photon counts from the background region. Assuming that the background x-ray photon density is uniform across the solar disk, we can express this as

$$z^{s,k}_i = \left(t^k_i - \frac{\theta^k}{360} N^{b,k}_{\gamma,i} \right) \frac{A^s_\odot}{A^b_\odot}, \qquad (4)$$

where t_i^k denotes the total number of photons detected in the bin i of the background region, $N_{\gamma,i}^{b,k}$ is the faint contribution from axions within the background annulus and $\theta^k/360$ is a correction factor for the cases in which bright sources are identified within our background selection. Furthermore, $A_\odot^s$ and $A_\odot^b$ represent the areas of the signal and background regions, respectively.

We assume independent Poisson statistics for each energy bin and calculate the likelihood for each module as

$$\mathcal{L}^k \propto \prod_i \frac{e^{-\lambda_i^k} \lambda_i^{k\, n_i^k}}{n_i^k!}. \quad (5)$$

In this analysis, n_i^k denotes the number of photons detected in the i bin of the energy spectrum of a given module. To derive our limit, we focus on the energy range from 4 to 11 keV and apply the prior $\Theta(g_{10}^4)$, where Θ is the Heaviside step function. We then integrate the Bayesian posterior probability density function (PDF) from zero to the point that includes 95% of the total PDF area. To obtain the combined bound shown in Fig. 1, we multiply the likelihoods of each module and follow the procedure described above applied to the total likelihood. The two modules yield similar bounds, the one from module A being slightly more stringent.

Our Letter considers various sources of systematic error, including the model uncertainties of the solar atmospheric magnetic field, which are the dominant contributors to the systematics, as well as uncertainties in the solar axion flux and the background of the NuSTAR detector. Overall, the combined effect of these uncertainties in our bound is calculated to be $^{+27.6\%}_{-21.2\%}$, which is further discussed in Supplemental Material [79].

Results and discussion—Using the statistical analysis outlined above, the NuSTAR solar axion observation data provides a constraint of $g_{a\gamma} \lesssim 7.3 \times 10^{-12}\ \mathrm{GeV}^{-1}$ at 95% CL on the axion-photon coupling strength $g_{a\gamma}$ for axion masses $m_a \lesssim 4 \times 10^{-7}$ eV. This limit is depicted in blue in the broader $m_a - g_{a\gamma}$ parameter space shown in Fig. 1. While NuSTAR's limits remain nearly constant for $m_a \lesssim 4 \times 10^{-7}$ eV, they weaken for higher axion masses due to the loss of coherence in the conversion probability, as described by Eq. (1), when the axion mass exceeds the plasma frequency at lower solar atmospheric heights. At low axion masses, the NuSTAR limit represents a significant improvement over the leading CAST constraint [10] (light red) and falls between the projected limits of future experiments, such as BabyIAXO [31] (dashed-dotted, with data collection scheduled to begin in 2028) and IAXO [41] (dashed, expected in the mid 2030s). For comparison, we also report the projected sensitivity of the ALPS-II laser propagation experiment at DESY [40] (dotted line) in Fig. 1. We note that the NuSTAR analysis presented here explores the $m_a - g_{a\gamma}$ parameter space with unprecedented sensitivity over a broad range of axion masses. The region explored in this project includes areas not accessible to any other current or near future axion experiments and probes large regions that could address the transparency hints [110].

Unlike haloscope experiments [11–39], helioscopes, including our Letter, do not assume axions to be dark matter, as the axion flux is inherently produced by the Sun. To maintain consistency, the luminosity associated with the axion flux must remain a small fraction of the total solar luminosity, to avoid significant energy loss due to escaping axions [111]. The measured solar neutrino flux and helioseismology observations place a constraint of $g_{10} \lesssim 4.1$ [112], which is well above the bounds reported here. In this regime, the theoretical precision of the axion flux is at the few-percent level [113], as outlined above, and therefore does not pose a significant systematic concern.

Acknowledgments—We gratefully acknowledge the support of the NuSTAR operations, software, and calibration teams in the execution and analysis of these observations. Our thanks also extend to Georg G. Raffelt, Jiří Štěpan, and T. O'Shea for insightful discussions. E. T., M. R., and M. T. are supported by the project "Theoretical Astroparticle Physics (TAsP)" funded by INFN and the "Grant for Internationalization" from the University of Torino. M. T. further acknowledges the research grant "Addressing Systematic Uncertainties in Searches for Dark Matter No. 2022F2843L" funded by MIUR. E. T. expresses gratitude to the University of Zaragoza for its hospitality during the initial phases of this work. This publication is based on work supported by COST Action COSMIC WISPers CA21106.

Data availability—The data that support the findings of this article are openly available [114].

[1] R. D. Peccei and H. R. Quinn, Phys. Rev. Lett. **38**, 1440 (1977).

[2] S. Weinberg, Phys. Rev. Lett. **40**, 223 (1978).

[3] F. Wilczek, Phys. Rev. Lett. **40**, 279 (1978).

[4] L. Abbott and P. Sikivie, Phys. Lett. **120B**, 133 (1983).

[5] J. Preskill, M. B. Wise, and F. Wilczek, Phys. Lett. **120B**, 127 (1983).

[6] M. Dine, W. Fischler, and M. Srednicki, Phys. Lett. **104B**, 199 (1981).

[7] M. Dine and W. Fischler, Phys. Lett. **120B**, 137 (1983).

[8] J. Jaeckel and A. Ringwald, Annu. Rev. Nucl. Part. Sci. **60**, 405 (2010).

[9] S. Moriyama, M. Minowa, T. Namba, Y. Inoue, Y. Takasu, and A. Yamamoto (SUMICO Collaboration), Phys. Lett. B **434**, 147 (1998).

[10] K. Altenmüller *et al.* (CAST Collaboration), Phys. Rev. Lett. **133**, 221005 (2024).

[11] S. J. Asztalos *et al.*, Phys. Rev. Lett. **104**, 041301 (2010).

[12] N. Du *et al.*, Phys. Rev. Lett. **120**, 151301 (2018).
[13] T. Braine *et al.*, Phys. Rev. Lett. **124**, 101303 (2020).
[14] C. Bartram *et al.* (ADMX Collaboration), Phys. Rev. Lett. **127**, 261803 (2021).
[15] C. Boutan *et al.*, Phys. Rev. Lett. **121**, 261302 (2018).
[16] C. Bartram *et al.*, Rev. Sci. Instrum. **94**, 044703 (2023).
[17] C. Hagmann, P. Sikivie, N. S. Sullivan, and D. B. Tanner, Phys. Rev. D **42**, 1297 (1990).
[18] L. Zhong *et al.*, Phys. Rev. D **97**, 092001 (2018).
[19] K. M. Backes *et al.*, Nature (London) **590**, 238 (2021).
[20] M. J. Jewell *et al.* (HAYSTAC Collaboration), Phys. Rev. D **107**, 072007 (2023).
[21] S. Lee, S. Ahn, J. Choi, B. R. Ko, and Y. K. Semertzidis, Phys. Rev. Lett. **124**, 101802 (2020).
[22] J. Jeong, S. W. Youn, S. Bae, J. Kim, T. Seong, J. E. Kim, and Y. K. Semertzidis, Phys. Rev. Lett. **125**, 221302 (2020).
[23] O. Kwon *et al.* (CAPP Collaboration), Phys. Rev. Lett. **126**, 191802 (2021).
[24] Y. Lee, B. Yang, H. Yoon, M. Ahn, H. Park, B. Min, D. L. Kim, and J. Yoo, Phys. Rev. Lett. **128**, 241805 (2022).
[25] J. Kim *et al.*, Phys. Rev. Lett. **130**, 091602 (2023).
[26] A. K. Yi *et al.*, Phys. Rev. Lett. **130**, 071002 (2023).
[27] B. Yang, H. Yoon, M. Ahn, Y. Lee, and J. Yoo, Phys. Rev. Lett. **131**, 081801 (2023).
[28] Y. Kim *et al.*, Phys. Rev. Lett. **133**, 051802 (2024).
[29] S. Ahn *et al.*, Phys. Rev. X **14**, 031023 (2024).
[30] A. Quiskamp, Ben T. McAllister, P. Altin, E. N. Ivanov, M. Goryachev, and M. E. Tobar, Sci. Adv. **8**, eabq3765 (2022).
[31] A. Quiskamp, Ben T. McAllister, P. Altin, E. N. Ivanov, M. Goryachev, and M. E. Tobar, Phys. Rev. Lett. **132**, 031601 (2024).
[32] B. T. McAllister, G. Flower, E. N. Ivanov, M. Goryachev, J. Bourhill, and M. E. Tobar, Phys. Dark Universe **18**, 67 (2017).
[33] D. Alesini *et al.*, Phys. Rev. D **99**, 101101 (2019).
[34] D. Alesini *et al.*, Phys. Rev. D **103**, 102004 (2021).
[35] R. Di Vora *et al.*, Phys. Rev. D **108**, 062005 (2023).
[36] J. A. Devlin *et al.*, Phys. Rev. Lett. **126**, 041301 (2021).
[37] J. L. Ouellet *et al.*, Phys. Rev. Lett. **122**, 121802 (2019).
[38] C. P. Salemi *et al.*, Phys. Rev. Lett. **127**, 081801 (2021).
[39] N. Crisosto, P. Sikivie, N. S. Sullivan, D. B. Tanner, J. Yang, and G. Rybka, Phys. Rev. Lett. **124**, 241101 (2020).
[40] R. Bähre *et al.*, J. Instrum. **8**, T09001 (2013).
[41] E. Armengaud *et al.* (IAXO Collaboration), J. Cosmol. Astropart. Phys. 06 (2019) 047.
[42] E. Armengaud *et al.*, J. Instrum. **9**, T05002 (2014).
[43] P. Sikivie, Phys. Rev. Lett. **51**, 1415 (1983).
[44] S. Tsuneta *et al.*, Sol. Phys. **136**, 37 (1991).
[45] E. D. Carlson and L.-S. Tseng, Phys. Lett. B **365**, 193 (1996).
[46] I. G. Hannah, G. J. Hurford, H. S. Hudson, R. P. Lin, and K. van Bibber, Astrophys. J. Lett. **659**, L77 (2007).
[47] I. G. Hannah, H. S. Hudson, G. J. Hurford, and R. P. Lin, Astrophys. J. **724**, 487 (2010).
[48] H. S. Hudson *et al.*, in *Proceedings of the 4th Hinode Science Meeting: Unsolved Problems and Recent Insights*, Astronomical Society of the Pacific Conference Series Vol. 455 (Astronomical Society of the Pacific (ASP), San Francisco, 2012), p. 25.
[49] F. A. Harrison *et al.*, Astrophys. J. **770**, 103 (2013).
[50] H.-J. Li, J.-G. Guo, X.-J. Bi, S.-J. Lin, and P.-F. Yin, Phys. Rev. D **103**, 083003 (2021).
[51] H.-J. Li, X.-J. Bi, and P.-F. Yin, Chin. Phys. C **46**, 085105 (2022).
[52] C. S. Reynolds, M. C. David Marsh, H. R. Russell, A. C. Fabian, R. Smith, F. Tombesi, and S. Veilleux, Astrophys. J. **890**, 59 (2020).
[53] A. Abramowski *et al.*, Phys. Rev. D **88**, 102003 (2013).
[54] M. Ajello *et al.*, Phys. Rev. Lett. **116**, 161101 (2016).
[55] J. Davies, M. Meyer, and G. Cotter, Phys. Rev. D **107**, 083027 (2023).
[56] S. Jacobsen, T. Linden, and K. Freese, J. Cosmol. Astropart. Phys. 10 (2023) 009.
[57] M. Xiao, K. M. Perez, M. Giannotti, O. Straniero, A. Mirizzi, Brian W. Grefenstette, Brandon M. Roach, and Melania Nynka, Phys. Rev. Lett. **126**, 031101 (2021).
[58] O. Ning and B. R. Safdi, Phys. Rev. Lett. **134**, 171003 (2025).
[59] C. Dessert, D. Dunsky, and B. R. Safdi, Phys. Rev. D **105**, 103034 (2022).
[60] C. Dessert, A. J. Long, and B. R. Safdi, Phys. Rev. Lett. **128**, 071102 (2022).
[61] D. Noordhuis, A. Prabhu, S. J. Witte, A. Y. Chen, F. Cruz, and C. Weniger, Phys. Rev. Lett. **131**, 111004 (2023).
[62] C. Dessert, J. W. Foster, and B. R. Safdi, Phys. Rev. Lett. **125**, 261102 (2020).
[63] S. Hoof and L. Schulz, J. Cosmol. Astropart. Phys. 03 (2023) 054.
[64] C. A. Manzari, Y. Park, B. R. Safdi, and I. Savoray, Phys. Rev. Lett. **133**, 211002 (2024).
[65] J. W. Foster, S. J. Witte, M. Lawson, T. Linden, V. Gajjar, C. Weniger, and B. R. Safdi, Phys. Rev. Lett. **129**, 251102 (2022).
[66] R. A. Battye, M. J. Keith, J. I. McDonald, S. Srinivasan, B. W. Stappers, and P. Weltevrede, Phys. Rev. D **108**, 063001 (2023).
[67] M. Escudero, C. K. Pooni, M. Fairbairn, D. Blas, X. Du, and David J. E. Marsh, Phys. Rev. D **109**, 043018 (2024).
[68] P. J. Fox, N. Weiner, and H. Xiao, Phys. Rev. D **108**, 095043 (2023).
[69] G. Raffelt, Astrophysical axion bounds, in *Axions: Theory, Cosmology, and Experimental Searches* (Springer, Berlin, Heidelberg, 2008), pp. 51–71.
[70] P. Carenza, M. Giannotti, J. Isern, A. Mirizzi, and O. Straniero, Phys. Rep. **1117**, 1 (2025).
[71] G. Raffelt and L. Stodolsky, Phys. Rev. D **37**, 1237 (1988).
[72] K. van Bibber, P. M. McIntyre, D. E. Morris, and G. G. Raffelt, Phys. Rev. D **39**, 2089 (1989).
[73] M. Rempel, Astrophys. J. **789**, 132 (2014).
[74] A. Vögler, S. Shelyag, M. Schüssler, F. Cattaneo, T. Emonet, and T. Linde, Astron. Astrophys. **429**, 335 (2005).
[75] M. Rempel, M. Schüssler, and M. Knölker, Astrophys. J. **691**, 640 (2009).

[76] J. Trujillo Bueno, N. Shchukina, and A. Asensio Ramos, Nature (London) **430**, 326 (2004).

[77] T. del Pino Aleman, J. Trujillo Bueno, J. Stepan, and N. Shchukina, Astrophys. J. **863**, 164 (2018).

[78] Z. Mikić *et al.*, Nat. Astron. **2**, 913 (2018).

[79] See Supplemental Material at http://link.aps.org/supplemental/10.1103/18sn-hxtb, for further details, explanations, and figures related to the analysis methods and procedures used in this Letter, which includes Refs. [80–95] in addition to those cited in the main Letter.

[80] J. N. Bahcall, W. F. Huebner, S. H. Lubow, P. D. Parker, and R. K. Ulrich, Rev. Mod. Phys. **54**, 767 (1982).

[81] E. Arik *et al.* (CAST Collaboration), J. Cosmol. Astropart. Phys. 02 (2009) 008.

[82] B. W. Lites *et al.*, Astrophys. J. **672**, 1237 (2008).

[83] R. Kariyappa, E. E. DeLuca, S. H. Saar, L. Golub, L. Damé, A. A. Pevtsov, and B. A. Varghese, Astron. Astrophys. **526**, A78 (2011).

[84] HEASARC, NuSTAR QuickPlots: A Diagnostic Plotting Tool for NuSTAR Data, NASA HEASARC/Caltech (2021), https://heasarc.gsfc.nasa.gov/docs/nustar/analysis/.

[85] B. W. Grefenstette *et al.*, Astrophys. J. **826**, 20 (2016).

[86] A. J. Dessler, J. Geophys. Res. (1896–1977) **64**, 713 (1959).

[87] M. Perri *et al.*, The NuSTAR Data Analysis Software Guide. Version 1.9.7 (2021), https://heasarc.gsfc.nasa.gov/docs/nustar/analysis/.

[88] D. R. Wik *et al.*, Astrophys. J. **792**, 48 (2014).

[89] S. Rossland *et al.*, Astron. J. **166**, 20 (2023).

[90] M. Arik *et al.* (CAST Collaboration), Phys. Rev. Lett. **107**, 261302 (2011).

[91] M. Arik *et al.* (CAST Collaboration), Phys. Rev. Lett. **112**, 091302 (2014).

[92] CAST Collaboration, Nat. Phys. **13**, 584 (2017).

[93] K. Zioutas, S. Andriamonje, V. Arsov *et al.*, Phys. Rev. Lett. **94**, 121301 (2005).

[94] A. Ayala, I. Domínguez, M. Giannotti, A. Mirizzi, and O. Straniero, Phys. Rev. Lett. **113**, 191302 (2014).

[95] M. J. Dolan, F. J. Hiskens, and R. R. Volkas, J. Cosmol. Astropart. Phys. 10 (2022) 096.

[96] P. Riley, J. A. Linker, Z. Mikić, R. Lionello, S. A. Ledvina, and J. G. Luhmann, Astrophys. J. **653**, 1510 (2006).

[97] V. De La Luz, A. Lara, E. Mendoza, and M. Shimojo, Geofis. Int. **47**, 197 (2008).

[98] J. E. Vernazza, E. H. Avrett, and R. Loeser, Astrophys. J. Suppl. Ser. **45**, 635 (1981).

[99] A. H. Gabriel, Phil. Trans. R. Soc. A **281**, 339 (1976).

[100] J. T. Schmelz, D. V. Reames, R. von Steiger, and S. Basu, Astrophys. J. **755**, 33 (2012).

[101] E. Caffau, H.-G. Ludwig, M. Steffen, B. Freytag, and P. Bonifacio, Sol. Phys. **268**, 255 (2011).

[102] K. Lodders, H. Palme, and H.-P. Gail, Landolt Börnstein **4B**, 712 (2009).

[103] K. P. Dere, E. Landi, H. E. Mason, B. C. Monsignori Fossi, and P. R. Young, Astron. Astrophys. Suppl. Ser. **125**, 149 (1997).

[104] G. Del Zanna, K. P. Dere, P. R. Young, and E. Landi, Astrophys. J. **909**, 38 (2021).

[105] M. J. Berger *et al.*, NIST standard reference database 8 (XGAM) (2010), https://www.nist.gov/srd/xcom.

[106] S. Paterson, I. G Hannah, B. W Grefenstette, H. S Hudson, S. Krucker, L. Glesener, S. M White, and D. M Smith, Mon. Not. R. Astron. Soc. **528**, 6398 (2024).

[107] S. Andriamonje *et al.* (CAST Collaboration), J. Cosmol. Astropart. Phys. 04 (2007) 010.

[108] K. A. Arnaud, in Astronomical Data Analysis SoKware and Systems V, editied by G. H. Jacoby and J. Barnes (1999), Vol. 101.

[109] N. F. Brejnholt *et al.*, in *Space Telescopes and Instrumentation 2012: Ultraviolet to Gamma Ray*, edited by T. Takahashi, S. S. Murray, and J.-W. A. den Herder, International Society for Optics and Photonics Vol. 8443 (SPIE, Amsterdam, Netherlands, 2012), p. 84431Y.

[110] M. Meyer, D. Horns, and M. Raue, Phys. Rev. D **87**, 035027 (2013).

[111] H. Schlattl, A. Weiss, and G. Raffelt, Astropart. Phys. **10**, 353 (1999).

[112] N. Vinyoles, A. Serenelli, F. L. Villante, S. Basu, J. Redondo, and J. Isern, J. Cosmol. Astropart. Phys. 10 (2015) 015.

[113] S. Hoof, J. Jaeckel, and L. J. Thormaehlen, J. Cosmol. Astropart. Phys. 09 (2021) 006.

[114] The data and analysis codes have been made available at https://github.com/elisabm99/nustar-helioscope.